




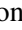


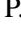


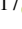










Observation of solar energetic particles with Metis on board Solar Orbiter on February 25, 2023

C. Grimani^{1,2}, M. Fabi^{1,2}, A. Persici^{3,4}, F. Sabbatini^{1,2}, M. Villani^{1,2}, F. Frassati⁵, E. Antonucci⁵, M. Pancrazzi⁵, D. Telloni⁵, P. Kühl⁶, J. Rodríguez-Pacheco⁷, R. F. Wimmer-Schweingruber⁶, V. Andretta⁸, P. Chioetto^{9,10}, V. Da Deppo⁹, S. Gissot¹¹, G. Jerse¹², M. Messerotti¹², G. Naletto^{13,10}, C. Plainaki¹⁴, M. Romoli^{15,16}, D. Spadaro¹⁷, M. Stangalini¹⁴, L. Teriaca¹⁸, M. Uslenghi¹⁹, L. Abbo⁵, A. Burtovoi^{15,16}, F. Landini⁵, G. Nicolini⁵, G. Russano⁸, C. Sasso⁸, and R. Susino⁵

(Affiliations can be found after the references)

Received 29 January 2024 / Accepted 2 March 2024

ABSTRACT

Context. The Solar Orbiter Metis coronagraph captures images of the solar corona in both visible (VL) and ultraviolet (UV) light. Tracks ascribable to the passage of galactic and solar particles appear in the Metis images. An algorithm implemented in the Metis processing electronics allows us to separate the pixels fired by VL photons from those crossed by high-energy particles. These spurious pixels are stored in cosmic-ray matrices that can be visually analyzed for particle monitoring deep into the spacecraft's interior. This algorithm has been enabled for the VL instrument only, since the process of separating the particle tracks from pixels fired by photons in the UV images was shown to be quite challenging with respect to a quantitative analysis.

Aims. This work is aimed at studying galactic cosmic rays (GCRs) and solar energetic particles (SEPs) with the Metis cosmic-ray matrices in February 2023.

Methods. We compared a visual analysis of Metis cosmic-ray matrices gathered on February 22, 2023, with GCRs only, and on February 25, 2023 with both GCRs and SEPs, to Monte Carlo simulations of the VL instrument during the same days.

Results. We estimated the solar modulation parameter associated with the GCR proton energy spectrum in February 2023. We show that Metis plays the role of monitoring galactic and solar protons. The Metis particle observations are used for the diagnostics of the VL instrument performance and to study the spacecraft inner charging from solar minimum towards the next solar maximum. These achievements have been attained with the benefit of the joint observations of Metis, the Energetic Particle Detector/High Energy Telescope, and near-Earth and Earth-based instruments.

Key words. instrumentation: detectors – Sun: particle emission – cosmic rays

1. Introduction

The ESA/NASA Solar Orbiter spacecraft (S/C, Müller et al. 2020; García Marirrodriga et al. 2021) was launched on February 10, 2020 at 4:03 UT from Cape Canaveral (Florida, USA) during the minimum of solar activity between solar cycles 24 and 25. Since then, the satellite has orbited the Sun between 0.28 AU and 1 AU close to the ecliptic plane. Metis is the Solar Orbiter coronagraph (Antonucci et al. 2020; Romoli et al. 2021), aimed at imaging the solar corona in visible (VL, in the range 580–640 nm) and ultraviolet light (UV, in a ≈ 20 nm band around the 121.6 nm Lyman- α line). Monte Carlo simulations (Vlachoudis 2009; Battistoni et al. 2014; Böhlen et al. 2014) performed for the Metis diagnostics (Telloni et al. 2016; Grimani et al. 2021, 2023a) have shown that only particles of galactic and solar origin with energies above tens of MeV penetrate into or interact in the Solar Orbiter S/C. Galactic cosmic rays (GCRs) lie in this energy range and consist of approximately: 90% protons, 8% helium nuclei, 1% electrons, and 1% nuclei with $Z \geq 3$, where the percentages refer to the proportion of individual particle numbers to the total (Simpson 1983; Papini et al. 1996). Solar energetic particles (SEPs) consist of approximately 99% of protons and rarely present energies well above tens of MeV (Reames 2021).

However, when this is indeed the case, the overall flux of particles incident on the Solar Orbiter S/C may increase by several orders of magnitude in less than half an hour for events that are magnetically well connected to the point of observations.

An algorithm meant for the VL instrument diagnostics, described in detail in Grimani et al. (2021, and references therein), separates the pixels fired by VL photons from those traversed by high-energy particles due to the large ionization energy losses of charged particle with respect to the energy released by photons in the sensitive part of the instrument. The spurious pixels fired by charged particles and the noisy pixels are stored in cosmic-ray matrices.

We carried out a visual analysis of cosmic-ray matrices gathered in February 2023 with particle tracks ascribable to GCRs only. The results of this study have been compared to those obtained with an analogous work carried out for the years 2020 and 2022 (Grimani et al. 2021, 2023a). These analyses give us the opportunity to verify if the number of spurious pixels (observed over time) appears consistent with Monte Carlo simulations based on particle energy spectra estimated according to the increasing solar modulation recorded after the mission launch. We may also see whether any variation in the instrument's performance is observed. In addition, for the first time,

we have had the opportunity to study a sudden increase in spurious pixels in the Metis images due to the occurrence of a gradual SEP event (Reames 2021, 2023) on February 25, 2023.

The monitoring of the number of particles reaching the inner parts of the S/C provides important clues on deep charging and instrument performance associated with high-energy particles by correlating measurements carried out outside the S/C with their effects deep into the satellite.

In Sect. 2, we illustrate the characteristics of the Metis VL images. In Sect. 3, the trend of the solar activity after the Solar Orbiter launch and the GCR energy spectra modulation are discussed. In Sect. 4, the evolution of the SEP event dated February 24–25, 2023 is presented. The solar eruption and coronal mass ejection (CME) associated with the SEP event are also briefly described. In Sect. 5, the results of the visual analysis of cosmic-ray matrices gathered in February 2023 with GCRs only are compared to those obtained in May 2020 and May 2022. We also study the increase in particle tracks in the Metis cosmic-ray matrices during the decay phase of the SEP event dated February 24–25, 2023. Finally, in Sect. 6, we report the results of Monte Carlo simulations of GCR and SEP particles in the cosmic-ray matrices on February 22 and February 25, 2023, followed by a comparison of the simulation outcomes to observations.

2. Metis images of the solar corona

Metis observes the solar corona from $1.7 R_{\odot}$ through $9 R_{\odot}$ in the range 580–640 nm and in the HI Lyman- α line at 121.6 nm (for a detailed description of the instrument see Antonucci et al. 2020; Fineschi et al. 2020). The coronagraph is mounted on one side of the Solar Orbiter S/C. A sketch of the instrument and satellite geometries built with Flair¹ (Vlachoudis 2009) is reported in Fig. 1. The S/C structure, thrusters, fuel tanks, and the SPICE, STIX, EUI, and PHI instruments (García Marirrodriga et al. 2021, and references therein) are shown. The Metis VL instrument consists of a VL camera with an active CMOS (CMOSIS ISPHI Rev. B developed by CMOSIS Imaging sensor, now AMS, Belgium) segmented in 4.1943×10^6 pixels of $10 \mu\text{m} \times 10 \mu\text{m} \times 4.5 \mu\text{m}$ dimensions. The geometrical factor of each pixel is $401 \mu\text{m}^2 \text{sr}$ (Sullivan 1971). The detailed design of the UV detector is illustrated in Uslenghi et al. (2017) and Schühle et al. (2018). It is worthwhile to point out that when the Metis VL and UV instruments are used for particle observations, each pixel of each image plays the role of a small detector. The lower limit to the single pixel efficiency of the VL instrument (defined as the ratio of fired pixels to the total number of pixels along the particle tracks) of 0.94 ± 0.02 was set by using a sample of oblique tracks firing more than three pixels (Grimani et al. 2021).

In principle, both Metis VL and UV instruments could be used for GCR and SEP observations. However, the separation of spurious from genuine signals in the pixels of the UV images appeared unfeasible for a quantitative analysis of particle tracks (see also Grimani et al. 2023a). As a result, in the following, we focus on the analysis of the cosmic-ray matrices of the VL instrument only.

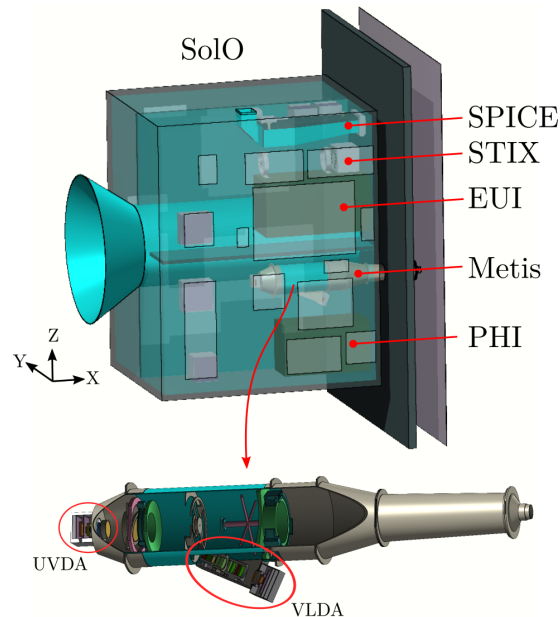


Fig. 1. Solar Orbiter geometrical model. Remote sensing instruments and electronic boxes are visible. The magnified image of Metis shows the VL (VLDA) and UV (UVDA) detector assemblies.

3. Solar activity and galactic cosmic-ray modulation since February 2020 for Solar Orbiter

In our previous works (Grimani et al. 2021, 2023a), we have shown that GCR flux modulation models optimized with data gathered near Earth at 1 AU can be used for Solar Orbiter for the first part of the mission before the S/C will lift out of the ecliptic. In particular, we adopted the Gleeson and Axford model (G&A; Gleeson & Axford 1968) to estimate the GCR energy spectra needed to simulate the particle tracks observed in the Metis cosmic-ray matrices (see Grimani et al. 2021). This model correlates the cosmic-ray intensity in the inner heliosphere to interstellar energy spectra through a solar modulation parameter (ϕ) that allows us to take into account diffusion, convection, and continuous energy losses of cosmic rays propagating from the interstellar medium to the point of observations. For global solar magnetic field positive polarity epochs, such as that encountered by Solar Orbiter up to the present time, the G&A model has been found to aptly reproduce the GCR measurements carried out at 1 AU in the energy range from tens of MeV to hundreds of GeV (see Grimani et al. 2008; Armano et al. 2018).

For this work, we have tested the reliability of the model with proton data gathered on board the International Space Station (ISS) with the magnetic spectrometer AMS-02 experiment. We have considered these measurements, available up to 2019, because they are affected by uncertainties of a few percent, although the data lie in the energy range above 450 MeV. An agreement within 10% (Aguilar et al. 2021; Grimani et al. 2023a) has been found between the measurements and model.

The solar modulation parameter increases with solar activity and varies with different particle interstellar spectra adopted for the calculation. In order to use the solar modulation parameter² estimated by Usoskin et al. (2011, 2017), the proton interstellar spectrum by Burger et al. (2000) must be considered. In Fig. 2, using the sunspot number as a proxy of solar activity (Brehm et al. 2021), we report the solar modulation parameter

¹ Flair is a python based graphical front-end interface of the FLUKA Monte Carlo program. A module of Flair, call geoedit (geometry editor) enables the building and debugging of complex combinatorial geometries: <https://flair.web.cern.ch/flair/>

² See http://cosmicrays.oulu.fi/phi/Phi_mon.txt

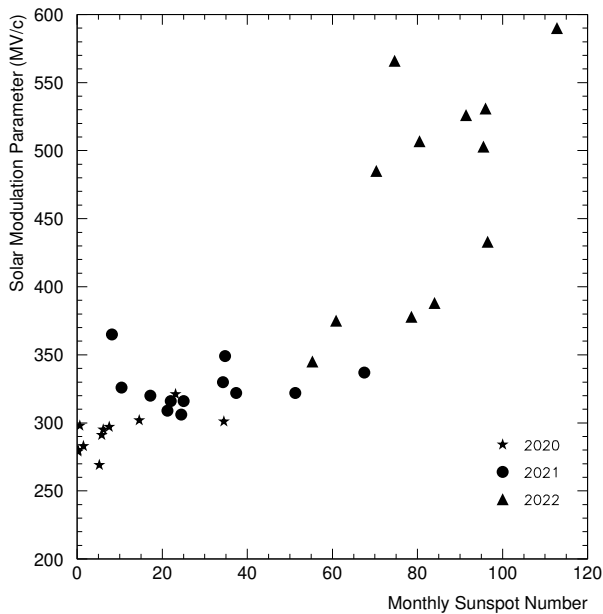


Fig. 2. Monthly sunspot number and solar modulation parameter from the Solar Orbiter launch in February 2020 through December 2022.

after the Solar Orbiter launch as a function of the monthly sunspot number³ (see Clette et al. 2014, for details about sunspot number calibration). It is possible to notice that the solar activity remained relatively low during the first two years of the mission while rapidly increased in 2022. The solar modulation parameter is not available for the year 2023 up to present time, but the sunspot number further increased beyond 120 during the first two months of 2023 (see also Adriani et al. 2023, for clues about cosmic-ray proton and electron flux modulation during the first months of 2023).

In this work we focus on GCR proton modulation only. In Grimani et al. (2023a), we demonstrated that the number of tracks in the cosmic-ray matrices ascribable to primary and secondary particles generated by galactic nuclei and electrons is numerically equivalent to the missing number of tracks due to pixel and on-board algorithm inefficiencies ($\approx 35\%$). In other words, we found that the number of tracks in the Metis cosmic-ray matrices is numerically equivalent to the number of primary and secondary particles associated with incident protons only. Monte Carlo simulations are used in the following to show that this hypothesis holds also during the increasing part of the solar cycle 25.

In Fig. 3, we report the average proton flux measured on board Solar Orbiter in different energy ranges by the two units constituting the High Energy Telescope (HET) instrument of the Energetic Particle Detector (EPD; Rodríguez-Pacheco et al. 2020). The two EPD/HET units point in the sun/antisun direction along the average Parker spiral and out of the ecliptic for a total of four viewing directions. The shown measurements were carried out during the Bartels rotation (BR) 2585. We recall that Bartels rotations are 27-day periods defined as complete rotations of the Sun viewed from Earth. Day 1 of rotation 1 was arbitrarily fixed to February 8, 1832. The energy range between 80 and 90 MeV (light blue in Fig. 3) is populated at steady state by particles of galactic origin. In addition to the GCR background, it is possible to notice the effects of three modest SEP

events that started on February 18, February 24 and February 25, 2023. The main increase in particles in the energy range >90 MeV, that typically give the main contribution to the inner S/C charging and to the tracks found in the Metis images (see for details Grimani et al. 2022, 2023b), is observed on February 24–25, 2023.

Metis cosmic-ray matrices were gathered between 14:00 UT and 15:00 UT on February 22 for GCR analysis and in the same interval of time on February 25 for SEP observations.

4. February 24–25, 2023 solar energetic particle event

The position of the Solar Orbiter S/C with respect to STEREO-A and Earth on February 24, 2023 at 21:00 UT is reported in Fig. 4. Solar Orbiter was at 0.77 AU from the Sun and at 0.54 AU from Earth (-32° in longitude with respect to Earth). As a result, the sequence of the events on the Sun at the origin of the SEP observations carried out with the EPD/HET and the Metis cosmic-ray matrices on February 25, 2023 was observed from a different perspective.

A filament eruption occurred within the active region (AR) 3229, situated in the north-west quadrant of the Sun (NOAA longitude: 18° , latitude: 25°), at approximately 20:03 UT on February 24, 2023 (refer to Fig. 5). The eruption was followed by an M3.7 flare starting around 20:07 UT and peaking at 20:26 according to soft X-ray measurements by GOES ($1\text{--}8 \text{ \AA}$; $1.55\text{--}12.4 \text{ keV}$)⁴. Soft X-rays in the range $1\text{--}5 \text{ keV}$ were observed to peak by the Solar Orbiter Spectrometer Telescope for Imaging X rays (STIX)⁵ approximately three minutes in advance with respect to GOES, due to the relative position of the two S/C. The event involved a halo CME, entering in the LASCO/C2 coronagraph field of view (FOV) at 20:36 (see Fig. 6, left panel). For the CME a speed of 1336 km s^{-1} ⁶ was estimated. The Type II radio burst detected by the e-Callisto system⁷ above 16 MHz (right panel of Fig. 6), starting around 20:22 UT, is the evidence of a propagating CME-driven shock upper in the solar corona believed to be at the origin of particle acceleration above tens of MeV. STEREO-A/WAVES data are also reported in the same figure below 16 MHz⁸.

The onset of the associated SEP event (the second event in Fig. 3) with a sharp increase and a gradual decay was observed by EPD/HET on board Solar Orbiter at 21:00 UT for 80–90 MeV protons and at 21:11 UT for 10–20 MeV protons. These timings were set when the overall proton flux recorded by the instrument increased by a factor of two above the background in the corresponding intervals of energy.

A new increase in solar protons, after a flare M6.35 on February 25, started at 21:01 UT for 80–90 MeV particles and at 22:50 UT for 10–20 MeV particles of the same day. As recalled above, Metis cosmic-ray matrices are available between 14:00 UT and 15:00 UT on February 25 during the decay phase of the second SEP event of the BR 2585 and before the onset of the third.

⁴ <https://www.ngdc.noaa.gov/stp/satellite/goes-r.html>
https://data.ngdc.noaa.gov/platforms/solar-space-observing-satellites/goes/goes18/12/data/xrsf-12-avg1m_science/2023/02/

⁵ <https://datacenter.stix.i4ds.net/> (Krucker et al. 2020)

⁶ https://cdaw.gsfc.nasa.gov/CME_list/UNIVERSAL_ver1/2023_02/univ2023_02.html

⁷ <http://soleil.i4ds.ch/solarradio/callistoQuicklooks/?date=20230224>

⁸ <http://stereo.space.umn.edu>

³ Data used here are publicly available at <http://www.sidc.be/silso/datafiles>

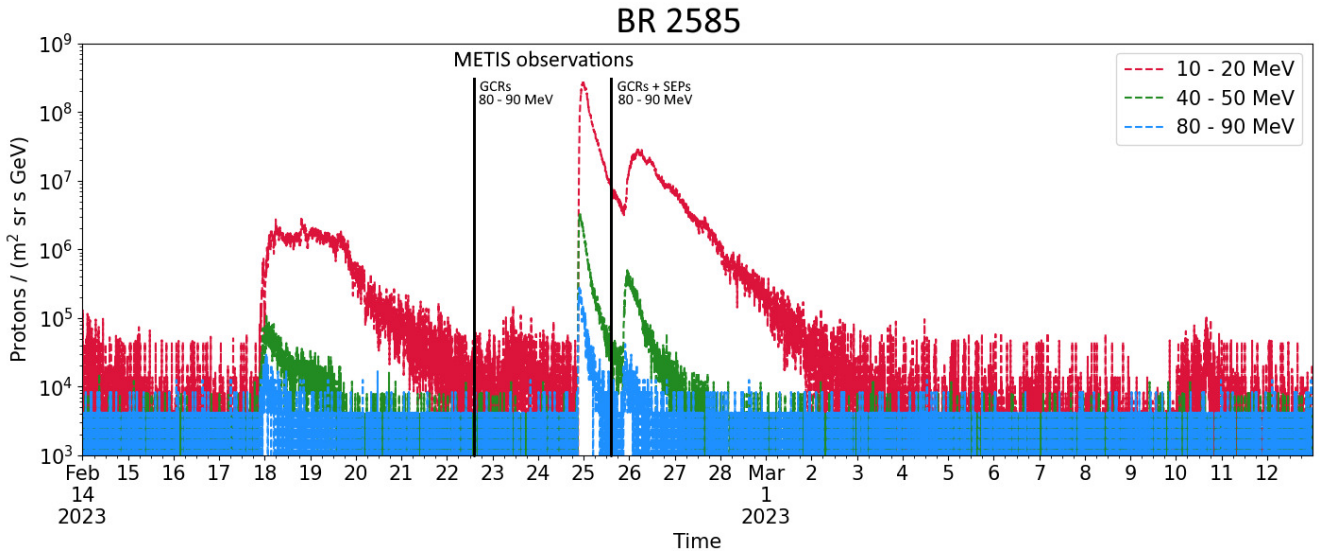


Fig. 3. Proton flux observed by the EPD/HET instrument on board Solar Orbiter during the BR 2585. Three SEP events are observed above the GCR background with onsets dated February 18, February 24 and February 25. Metis cosmic-ray matrices are available between 14:00 UT and 15:00 UT on February 22, before the onset of the second SEP event, and at the same time on February 25 during the SEP event (data availability is indicated by vertical thick black lines). GCRs only and GCRs+SEPs populate the energy bin between 80 and 90 MeV on February 22 and 25, respectively.

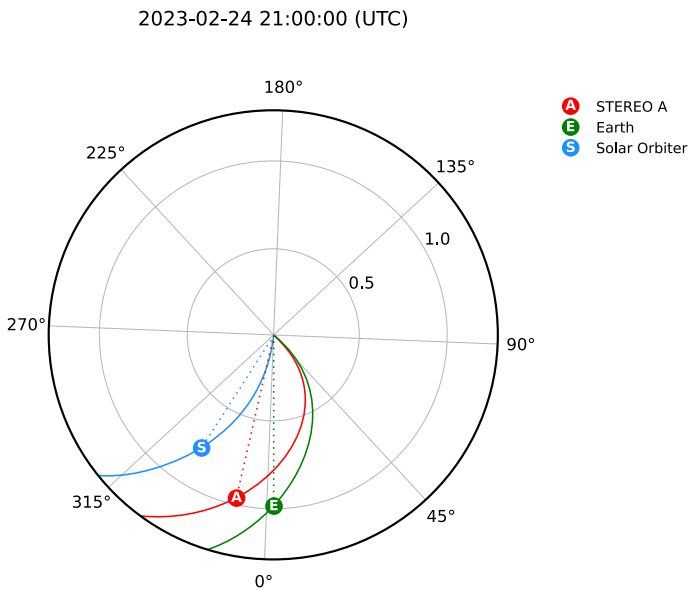


Fig. 4. View of the ecliptic plane from solar north on February 24, 2023 at 21:00 UT. The Parker spirals are shown at the positions of Solar Orbiter (S), Stereo A (A), and Earth (E). Solar Orbiter was at 0.77 AU from the Sun and at 0.54 AU from Earth. The image was obtained with the Solar MAGnetic Connection Haus tool (Gieseler et al. 2023), <https://solar-mach.github.io/>.

5. Galactic and solar particles in the Metis VL images

The analysis of GCR and SEP tracks in the Metis images is part of the diagnostics of the VL instrument. In this work, with the first quantitative Metis observation of SEPs, we have the opportunity to correlate the response of the instrument to both galactic and solar particle fluxes incident on the S/C.

The average number of tracks observed in three cosmic-ray matrices gathered on February 22 and three gathered on

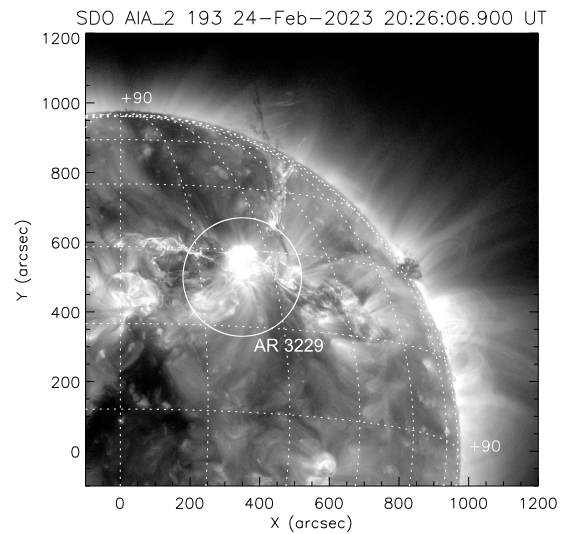


Fig. 5. Active region 3229 firing off an M3.7 flare and filament (SDO/AIA 193 Å) at 20:26 UT on February 24, 2023.

February 25 between 14.00 UT and 15.00 UT have been studied with a visual analysis. Only three out of eight cosmic-ray matrices available for each session were selected due to the large block of time needed for the visual analysis of each matrix. The cosmic-ray matrices consist of 12 frames of 30s exposure times apiece, for a total exposure time of 6 minutes. The visual analysis was carried out with the APViewer (described in detail in Grimani et al. 2021, and references therein) adapted to the new sets of images. Developed specifically for Metis using the Python programming language, the APViewer serves as a powerful tool for analyzing particle tracks in cosmic-ray matrices. This innovative software streamlines the process of visualizing and identifying cosmic-ray tracks while offering unique solutions to common challenges encountered with other tools. Unlike conventional tools tailored for FITS images,

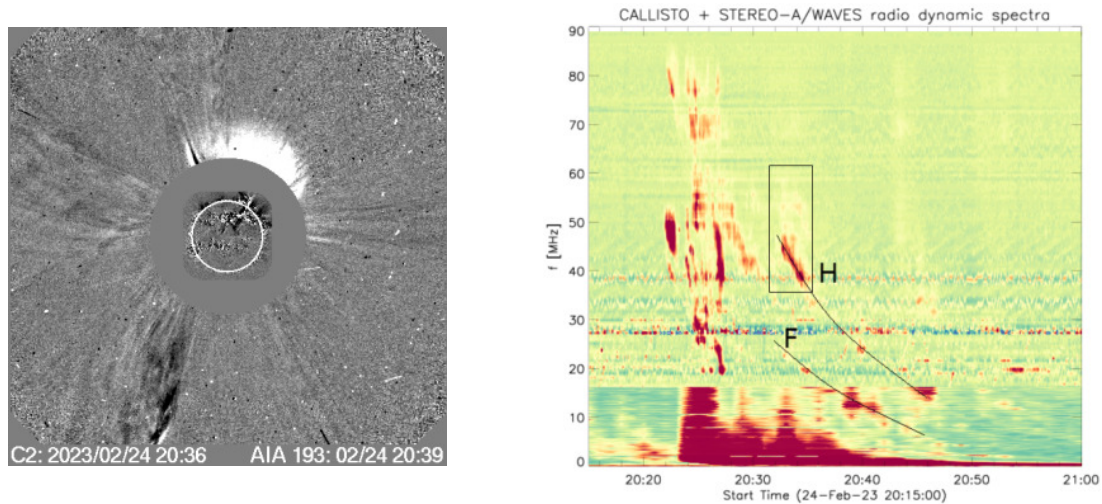


Fig. 6. Running difference image of the shock ahead the halo CME entering in the LASCO C2 FOV (left). The expanding front followed the filament eruption shown in Fig. 5 from the same AR. Type II radio burst observed with the e-Callisto system (ALASKA- HAARP, >16 MHz) combined with space-based STEREO-A/WAVES (<16 MHz) data (right). The fundamental (*F*) and harmonic (*H*) band, after 20:30 UT, are marked with black solid lines. The black rectangular border highlights the harmonic splitting.

the APViewer introduces several innovative features. Among its advanced functionalities, it allows for the visualization of the number of active pixels across multiple frames within an image, for instance. This capability plays a pivotal role in discerning cosmic-ray tracks from noisy pixels, thus facilitating more accurate identification of relevant features within the data. Additionally, the APViewer allows users to customize window sizes for track-specific analysis. These features collectively enhance the precision and efficiency of examining cosmic-ray tracks and their contextual surroundings. The performance of the VL instrument in 2023 has been compared to previous studies carried out in 2020 and 2022. To this end, it is important to point out that the Metis algorithm generating the cosmic-ray matrices has been used in all analyses with the same parameters reported in Grimani et al. (2021). The algorithm is activated occasionally to limit the data volume. Single, clusters and columns of noisy pixels appearing in more than two frames of each image were neglected in the analysis. These noisy pixels have been found to correspond to a fraction of about 10^{-5} of the total number of image pixel sample, consistently with prior analyses. In other words, the number of noisy pixels in the Metis VL images was not found to change during the first three years of the Solar Orbiter mission. The number of pixels fired by cosmic rays remained always below one order of magnitude in excess with respect to noisy pixels.

Particle tracks are classified on the basis of their topology. Straight tracks (single fired pixels appearing in only one frame out of 12 forming each image), slant tracks (firing more than one pixel along the main particle track), and “squares” (4 pixels forming a square, a small slant track with possible production of δ rays) are shown in Fig. 7. The particle tracks reconstructed with a generic viewer are compared to those obtained with the dedicated APViewer.

The total number of straight tracks, slant tracks and squares for the 2023 analysis are reported in Table 1 after normalization of data to 60-s exposure time. This normalization was needed for comparison with the analysis carried out in 2020 when the cosmic-ray matrices exposure time was of one minute. Analogous normalizations were carried out for the observations gathered in 2022 with 7 min exposure time. The 2023 average

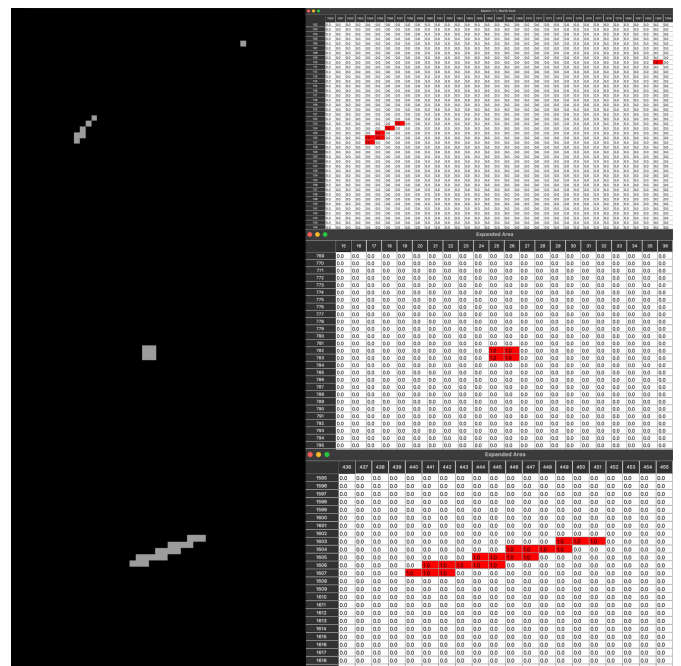


Fig. 7. Examples of particle tracks in the Metis VL instrument cosmic-ray matrices gathered in 2023. Left panel: outcomes of a viewer, not expressly dedicated to the analysis of Metis cosmic-ray matrices, for oblique and straight tracks (top figure), squares (middle figure) and slant track with several extra pixels possibly fired by secondary particles generated in the sensitive part of the detector (bottom figure). Right panel: same tracks reported in the left panel, but displayed with the APViewer developed specifically for the visual analysis of the Metis cosmic-ray matrices.

number of particle tracks of 120 ± 5 observed in 60 s appears drastically lower than previous observations. This is expected due to the increase in solar activity mainly during the last year. It is quite interesting to notice that the percentage of slant tracks with respect to straight tracks (of about 40%) has remained approximately constant through the solar cycle being primarily

Table 1. Metis cosmic-ray matrix GCR and SEP track average observations in February 2023 in comparison to GCR observations in 2020 and 2022.

	Straight	Slant	Squares	Total
May 2020 (GCRs)				
Average	188	79	4	271 ± 22
May 2022 (GCRs)				
Average	151	57	4	212 ± 6
February 2023 (GCRs)				
Average	83	36	1	120 ± 5
February 2023 (GCRs+SEPs)				
Average	108	51	2	161 ± 5

Notes. The uncertainties indicate the standard deviations from averages for each set of cosmic-ray matrices. Data gathered in 2022 and 2023 have been normalized to one minute exposure time for comparison with the previous analyses carried out in 2020. Examples of the track topologies are reported in Fig. 7.

associated with the isotropic spatial distribution of galactic cosmic rays. Conversely, the slant tracks ascribable to the passage of solar particles during the declining phase of the February 25, 2023 SEP event, were 60% of the straight tracks. Even if these two results are compatible within 1σ (15 slant tracks and 25 straight tracks estimated for SEP particles), this evidence may also indicate that the spatial distribution of hundreds of MeV solar particles is not exactly isotropic like that of galactic cosmic rays.

6. Monte Carlo simulations of galactic and solar particles in the Metis images

The results of the visual analysis of cosmic-ray matrices are compared in the following to Monte Carlo simulations of the VL instrument during the same days. Input GCR and SEP particle energy spectra are needed for the simulations. The G&A model for cosmic-ray proton modulation in February 2023 (solid line in Fig. 8) has been used with a solar modulation parameter of 650 MV c^{-1} . This value was reasonably set by following the data trend shown in Fig. 2 at the end of 2022 (590 MV c^{-1}) and because of a further increase in the solar activity recorded during the first two months of 2023 (Adriani et al. 2023). In Fig. 8, our best estimate of the proton energy spectrum in February 2023 (thick continuous line) is compared to the interstellar spectrum by Burger et al. (2000; dotted line) and to the modulated energy spectra obtained by assuming $\phi = 300 \text{ MV c}^{-1}$ (dot-dot-dot-dashed line), $\phi = 500 \text{ MV c}^{-1}$ (dot-dashed line), and $\phi = 800 \text{ MV c}^{-1}$ (dot-dot-dashed line).

We show here that by using $\phi = 650 \text{ MV c}^{-1}$ we are able to reconcile both GCR and GCR+SEP observations with simulations fairly well. The proton energy spectrum obtained with $\phi = 650 \text{ MV c}^{-1}$ has been parameterized as follows (see for details Armano et al. 2018):

$$F(E) = A (E + b)^{-\alpha} E^\beta \text{ protons}/(\text{m}^2 \text{ sr s GeV}), \quad (1)$$

where E is the particle kinetic energy in GeV. The parameters A , b , α , and β are given in Table 2. It is worthwhile to point out that

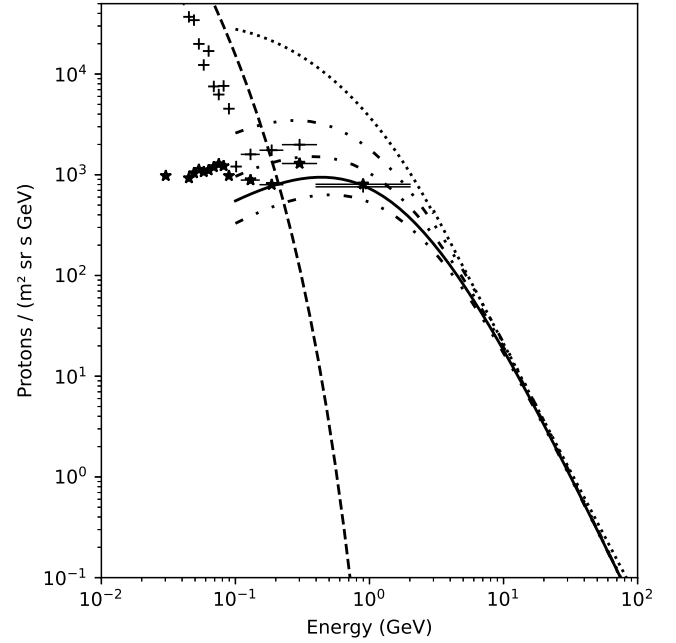


Fig. 8. Interstellar proton energy spectrum by Burger et al. (2000; dotted line) with our best prediction of the cosmic-ray proton energy spectrum in February 2023 (thick continuous line, $\phi = 650 \text{ MV c}^{-1}$). The modulated proton spectra obtained by assuming a solar modulation parameter of 300 MV c^{-1} (dot-dot-dot-dashed line), 500 MV c^{-1} (dot-dashed line) and 800 MV c^{-1} (dot-dot-dashed line) are shown for comparison. The solid stars (crosses) indicate the GCR (SEP) proton measurements carried out on February 22 (25), 2023 by the EPD/HET experiment. The tight line represents the PAMELA experiment observations during the decay phase of a weak SEP event dated December 14, 2006.

A is measured in protons/ $(\text{m}^2 \text{ sr s GeV}^{-\alpha+\beta+1})$, b in GeV while α and β are pure numbers.

In Fig. 8, the cosmic-ray proton energy spectrum predictions are compared to the proton differential flux measurements gathered by the EPD/HET instrument hosted on board Solar Orbiter on February 22, 2023 (solid stars). The crosses in Fig. 8 represent the solar proton flux measured by the same experiment between 14:00 UT and 15:00 UT on February 25. The SEP component is dominant up to 100 MeV, becomes comparable to the cosmic-ray flux up to hundreds of MeV and vanishes above 1 GeV.

In Fig. 8, we also show, for comparison, the proton flux observed by the satellite experiment PAMELA on December 14, 2006 (dashed line; Adriani et al. 2011) during the declining phase of a SEP event of intensity slightly higher than that studied here (dashed line). Monte Carlo simulations of the two SEP events are compared in the following (see also Grimani et al. 2023a).

For the MC simulation aimed at reproducing the GCR and SEP tracks in the Metis cosmic-ray matrices in February 2023, we adopted the CERN release of the FLUKA code (version 4.0.1)⁹ (Battistoni et al. 2014; Böhlen et al. 2014), which is a general purpose tool written in Fortran devoted to the calculation of particle transport and interaction with matter. As anticipated in Sect. 2, the geometries of the Solar Orbiter S/C and the Metis coronagraph have been built with Flair (Vlachoudis 2009) for FLUKA.

⁹ <https://fluka.cern>

Table 2. Galactic cosmic-ray proton energy spectrum parameters in February 2023 (see Eq. (1)).

Particle species	A protons/(m ² sr s GeV ^{-α+β+1})	b (GeV)	α	β
p	18 000.	1.40	3.66	0.87

Table 3. Number of tracks in the cosmic-ray matrices of the Metis VL instrument according to Monte Carlo (MC) simulations and observations during 60-s exposure time by considering primary protons.

	Number of tracks		$\phi_{\text{estimated}}$ (MV c ⁻¹)	ϕ_{real} (MV c ⁻¹)
	MC	Observed		
GCRs				
May 2020	276 ± 39 ± 17	271 ± 22	300	299
May 2022	242 ± 34 ± 16	212 ± 6	340	433
February 2023	118 ± 17 ± 11	120 ± 5	650	?
GCRs+SEPs				
February 25, 2023	143 ± 20 ± 12	161 ± 5		

Notes. Systematic and statistical uncertainties on the MC results are shown. As expected, a better agreement between particle track observations and MC simulations is found when the solar modulation parameter adopted for the estimate of the proton energy spectra used for the simulations (300 MV c⁻¹) is similar to the observed value (299 MV c⁻¹), as in 2020. The reliability of the solar modulation parameter estimate for February 2023 will be verified when the actual value will be available.

Particles traversing the Metis VL instrument pass through a varying amount of S/C and instrument material depending on their incidence direction on the S/C. Metis is set on one side of the Solar Orbiter S/C and, therefore, the minimum grammage of matter traversed by galactic and solar particles before reaching the instrument is about 1 g cm⁻². However, the active silicon CMOS of the VL camera is also shielded by the instrument material. Monte Carlo simulations indicate that below 90 MeV n⁻¹ protons and ions with an isotropic spatial distribution, do not produce tracks in the cosmic-ray matrices.

The simulations of the tracks of GCR protons in the Metis images for the years 2020-2023 and of solar protons on February 25, 2023 between 14:00 UT and 15:00 UT are reported in Table 3 normalized to 60-s exposure time for comparison with observations. The simulations are affected by systematic uncertainties of 10% associated with cosmic-ray proton models and 10% due to the FLUKA Monte Carlo program accuracy (Lechner et al. 2019) for a total of 14%.

Both systematic and statistical uncertainties on the simulation results are shown in the table. A very good agreement between observations and simulations was found in 2020 when the estimate of the solar modulation parameter was close to the observed value. In 2022 we set a lower limit to the solar modulation parameter of 340 MV c⁻¹. The actual value was later found of 433 MV c⁻¹, 83 MV c⁻¹ larger. Consistently, the simulations returned a higher number of GCR tracks than observed. For the month of February 2023 observations and simulations of GCR only are consistent with $\phi = 650$ MV c⁻¹. This solar modulation parameter allows us also to reconcile simulations and observations of the SEP tracks in addition to the GCR background in the Metis cosmic-ray matrices. The number of particle tracks associated with the SEP event for 60 s of exposure time is 41. The simulations return 25 tracks, in agreement with observations within slightly more than 1 σ .

In a previous study (Grimani et al. 2023a), we considered the decay phase of the SEP event observed by the PAMELA experiment on December 14, 2006. For this event we estimated

180 tracks in cosmic-ray matrices for the same exposure time. This PAMELA event was characterized by a proton flux higher by approximately a factor of 4 above tens of MeV and below 200 MeV with respect to the February 25, 2023 event. The present MC simulations appear consistent with this previous work.

Metis can be considered a proton monitor under different conditions of solar activity, if the particles that cross the VL images are numerically equivalent to those generated by protons in terms of primary and secondary particles. This actually seems to be the case on the basis of the results reported in Table 3. Simulations for the month of February 2023, near solar maximum, indicate that when galactic protons are considered as primary particles, the composition of particle tracks in the Metis cosmic-ray matrices consists of 69% protons, 21% e⁻, 4% π^- , 3% π^+ , 2% e⁺, and 1% μ^- . In Grimani et al. (2023a, and references therein,) we reported that in 2020 the proton component was at 80%, whereas in 2022, it was at 77%. Even though the percentage of galactic protons to the total number of particles decreases with increasing solar activity, possibly due to a smaller number of low-energy particles that are unlikely to interact in the S/C, protons remain by far the most abundant particles crossing the VL instrument of Metis and the total number of particles generated by protons appears in line with observations. If the solar modulation parameter in February 2023 was actually close to 650 MV c⁻¹, it would also indicate that the algorithm in the Metis electronics removes a sample of cosmic-ray tracks, equivalent to the contribution of the other components of GCRs, regardless of solar activity intensity (Grimani et al. 2021).

Metis is an even better proton monitor during SEP events when protons below 1 GeV dominate the total particle flux incident on the spacecraft and a small number of secondaries is produced deep inside the S/C. As a matter of fact, simulations indicate that during the decay phase of the February 25 SEP event the fraction of tracks ascribable to protons was of 92%, while only 8% of the total bulk of particle tracks was associated with secondary electrons.

7. Conclusions

We studied the response of the VL instrument of the Metis coronagraph on board Solar Orbiter to GCRs and SEPs after the S/C launch. Noisy pixels of the VL images have been found to constitute a fraction of about 10^{-5} of the total number of pixels over the years 2020–2023. The percentage of pixels fired by cosmic rays is approximately one order of magnitude larger, with an absolute number that has decreased by more than a factor of 2 (from 271 through 120 in 60-s exposure time) due to the increasing solar modulation during the last three years.

The decay phase of a modest SEP event was observed on February 25, 2023. Solar energetic particles were found to fire a fraction of 10^{-5} of the total number of pixels in the Metis VL images. This number increases by several orders of magnitude during medium-strong SEP events. Although this work is primarily intended for instrument diagnostics, we were also able to estimate the solar modulation parameter ($\phi = 650 \text{ MV c}^{-1}$) representative of the propagation of GCRs in the inner heliosphere in February 2023 with observations and Monte Carlo simulations. We note that to obtain the results presented in this paper, it was of paramount importance to benefit from the data gathered by Metis and EPD/HET instruments on board Solar Orbiter, in addition to near-Earth and Earth instruments.

Acknowledgements. Solar Orbiter is a space mission of international collaboration between ESA and NASA, operated by ESA. The Metis program is supported by the Italian Space Agency (ASI) under the contracts to the co-financing National Institute of Astrophysics (INAF): Accordi ASI-INAF N. I-043-10-0 and Addendum N. I-013-12-0/1, Accordo ASI-INAF N.2018-30-HH.0 and under the contracts to the industrial partners OHB Italia SpA, Thales Alenia Space Italia SpA and ALTEC: ASI-TASI N. I-037-11-0 and ASI-ATI N. 2013-057-I.0. Metis was built with hardware contributions from Germany (Bundesministerium für Wirtschaft und Energie (BMWi) through the Deutsches Zentrum für Luft- und Raumfahrt e.V. (DLR)), from the Academy of Science of the Czech Republic (PRODEX) and from ESA. The EPD/HET data up to 100 MeV are publicly available on the Solar Orbiter Archive (SOAR, <https://soar.esac.esa.int/soar/>). The data above 100 MeV were kindly provided by the EPD/HET Collaboration as a private communication. We also thank the EPD/HET Collaboration for useful discussions about proton observations gathered aboard Solar Orbiter and the PHI and EUI Collaborations for providing useful details about instrument geometries for S/C simulations. Finally, we are very grateful to Salvatore Mancuso of the Astrophysical Observatory of Torino (INAF, Italy) for useful discussions on STEREO-A radio observations.

References

- Adriani, O., Barbarino, G. C., Bazilevskaya, G. A., et al. 2011, *ApJ*, **742**, 102
 Adriani, O., Akaike, Y., Asano, K., et al. 2023, *PoS, ICRC2023*, 1253
 Aguilar, M., Cavasonza, L. A., Ambrosi, G., et al. 2021, *Phys. Rev. Lett.*, **127**, 271102
 Antonucci, E., Romoli, M., Andretta, V., et al. 2020, *A&A*, **642**, A10
 Armano, M., Audley, H., Baird, J., et al. 2018, *ApJ*, **854**, 113
 Battistoni, G., Boehlen, T., Cerutti, F., et al. 2014, *Joint International Conference on Supercomputing in Nuclear Applications + Monte Carlo*, 06005
 Böhlen, T. T., Cerutti, F., Chin, M. P. W., et al. 2014, *Nucl. Data Sheets*, **120**, 211
 Brehm, N., Bayliss, A., Christl, M., et al. 2021, *Nat. Geosci.*, **14**, 10
 Burger, R. A., Potgieter, M. S., & Heber, B. 2000, *J. Geophysical Res.: Space Phys.*, **105**, 27447
 Clette, F., Svalgaard, L., Vaquero, J. M., & Cliver, E. W. 2014, *Space. Sci. Rev.*, **186**, 35
 Fineschi, S., Naletto, G., Romoli, M., et al. 2020, *Exp. Astron.*, **49**, 239
 García Marínrodriga, C., Pacros, A., Strandmoe, S., et al. 2021, *A&A*, **646**, A121
 Gieseler, J., Dresing, N., Palmroos, C., et al. 2023, *Front. Astron. Space Sci.*, **9**, 384

- Gleeson, L. J., & Axford, W. I. 1968, *ApJ*, **154**, 1011
 Grimani, C., Fabi, M., Finetti, N., & Tombolato, D. 2008, *Int. Cosmic Ray Conf.*, **1**, 485
 Grimani, C., Andretta, V., Chioetto, P., et al. 2021, *A&A*, **656**, A15
 Grimani, C., Villani, M., Fabi, M., Cesarini, A., & Sabbatini, F. 2022, *A&A*, **666**, A38
 Grimani, C., Andretta, V., Antonucci, E., et al. 2023a, *A&A*, **677**, A45 (SO Nominal Mission Phase SI)
 Grimani, C., Fabi, M., Sabbatini, F., et al. 2023b, *Astrophys. Space Sci.*, **368**, 78
 Krucker, S., Hurford, G. J., Grimm, O., et al. 2020, *A&A*, **642**, A15
 Lechner, A., Auchmann, B., Baer, T., et al. 2019, *Phys. Rev. Accel. Beams*, **22**, 071003
 Müller, D., St. Cyr, O. C., Zouganelis, I., et al. 2020, *A&A*, **642**, A1
 Papini, P., Grimani, C., & Stephens, S. 1996, *Nuovo Cim. C*, **19**, 367
 Reames, D. V. 2021, *Gradual SEP Events* (Cham: Springer International Publishing), 97
 Reames, D. V. 2023, *Universe*, **9**, 466
 Rodríguez-Pacheco, J., Wimmer-Schweingruber, R. F., Mason, G. M., et al. 2020, *A&A*, **642**, A7
 Romoli, M., Antonucci, E., Andretta, V., et al. 2021, *A&A*, **656**, A32
 Schühle, U., Teriaca, L., Aznar Cuadrado, R., et al. 2018, in *Space Telescopes and Instrumentation 2018: Ultraviolet to Gamma Ray*, eds. J. W. A. den Herder, S. Nikzad, & K. Nakazawa, *SPIE Conf. Ser.*, **10699**, 1069934
 Simpson, J. A. 1983, *Ann. Rev. Nucl. Part. Sci.*, **33**, 323
 Sullivan, J. 1971, *Nucl. Instrum. Methods*, **95**, 5
 Telloni, D., Fabi, M., Grimani, C., & Antonucci, E. 2016, *AIP Conf. Proc.*, **1720**
 Uslenghi, M., Schühle, U. H., Teriaca, L., Heerlein, K., & Werner, S. 2017, in *SPIE Conf. Ser.*, ed. O. H. Siegmund, 10397, 103971K
 Usoskin, I. G., Bazilevskaya, G. A., & Kovaltsov, G. A. 2011, *J. Geophys. Res. (Space Phys.)*, **116**, A02104
 Usoskin, I. G., Gil, A., Kovaltsov, G. A., Mishev, A. L., & Mikhailov, V. V. 2017, *J. Geophys. Res. (Space Phys.)*, **122**, 3875
 Vlachoudis, V. 2009, in *International Conference on Mathematics, Computational Methods & Reactor Physics (M&C 2009)*, Saratoga Springs, New York, 790

¹ DiSPeA, University of Urbino Carlo Bo, Urbino, PU, Italy
 e-mail: catia.grimani@uniurb.it

² INFN, Florence, Italy

³ European Space Agency, ESAC, Camino Bajo del Castillo s/n, Villanueva de la Cañada, Madrid, Spain

⁴ Politecnico di Milano, Milano, Italy

⁵ INAF-Astrophysical Observatory of Torino, Torino, Italy

⁶ Institut für Experimentelle und Angewandte Physik, Christian-Albrechts-Universität zu Kiel, Kiel, Germany

⁷ Universidad de Alcalá, Space Research Group, 28805 Alcalá de Henares, Spain

⁸ INAF – Astronomical Observatory of Capodimonte, Naples, Italy

⁹ CNR-IFN, Via Trasea 7, 35131 Padova, Italy

¹⁰ CISAS, Centro di Ateneo di Studi e Attività Spaziali “Giuseppe Colombo”, via Venezia 15, 35131 Padova, Italy

¹¹ Solar-Terrestrial Centre of Excellence – SIDC, Royal Observatory of Belgium, Ringlaan -3- Av. Circulaire, 1180 Brussels, Belgium

¹² INAF – Astrophysical Observatory of Trieste, Trieste, Italy

¹³ Dip. di Fisica e Astronomia “Galileo Galilei”, Università di Padova, Via G. Marzolo 8, 35131 Padova, Italy

¹⁴ ASI – Italian Space Agency, Via del Politecnico snc, 00133 Rome, Italy

¹⁵ University of Florence, Physics and Astronomy Department, Largo E. Fermi 2, 50125 Florence, Italy

¹⁶ INAF – Arcetri Astrophysical Observatory, Largo Enrico Fermi 5, 50125 Florence, Italy

¹⁷ INAF-Astrophysical Observatory of Catania, Catania, Italy

¹⁸ MPS, Göttingen, Germany

¹⁹ INAF – Institute for Space Astrophysics and Cosmic Physics, Milan, Italy